
Since January 2020 Elsevier has created a COVID-19 resource centre with free information in English and Mandarin on the novel coronavirus COVID-19. The COVID-19 resource centre is hosted on Elsevier Connect, the company's public news and information website.

Journal of Controlled Release 346 (2022) 421–433

Contents lists available at ScienceDirect

Journal of Controlled Release

journal homepage: www.elsevier.com/locate/jconrel

Editorial

# Lung targeted liposomes for treating ARDS

Sivan Arber Raviv [a,1], Mohammed Alyan [a,b,1], Egor Egorov [a], Agam Zano [a], Moshit Yaskin Harush [a], Calvin Pieters [a], Hila Korach-Rechtman [a], Adi Saadya [a], Galoz Kaneti [a], Igor Nudelman [a], Shai Farkash [e], Ofri Doppelt Flikshtain [a], Lucy N. Mekies [a], Lilach Koren [a], Yoav Gal [c], Ella Dor [c], Janna Shainsky [a], Jeny Shklover [a], Yochai Adir [d], Avi Schroeder [a,*]

[a] The Louis Family Laboratory for Targeted Drug Delivery and Personalized Medicine Technologies, Department of Chemical Engineering, Technion - Israel Institute of Technology, Haifa 32000, Israel
[b] The Interdisciplinary Program for Biotechnology, Technion, Haifa, 3200003, Israel.
[c] Office Of Assistant Minister of Defense for CBRN Defense, Ministry of Defense, Tel-Aviv, Israel
[d] Pulmonary Division, Lady Davis, Carmel Medical Center, Faculty of Medicine, The Technion Institute of Technology, Haifa, Israel
[e] Department of Pathology, Emek Medical Center, Afula, Israel

ARTICLE INFO

*Keywords:*
Liposome
Pulmonary
ARDS
Covid-19
COPD
Lung inflammation
Mucus
Nanotechnology

ABSTRACT

Acute Respiratory Distress Syndrome (ARDS), associated with Covid-19 infections, is characterized by diffuse lung damage, inflammation and alveolar collapse that impairs gas exchange, leading to hypoxemia and patient' mortality rates above 40%. Here, we describe the development and assessment of 100-nm liposomes that are tailored for pulmonary delivery for treating ARDS, as a model for lung diseases. The liposomal lipid composition (primarily DPPC) was optimized to mimic the lung surfactant composition, and the drug loading process of both methylprednisolone (MPS), a steroid, and *N*-acetyl cysteine (NAC), a mucolytic agent, reached an encapsulation efficiency of 98% and 92%, respectively. In vitro, treating lipopolysaccharide (LPS)-stimulated RAW 264.7 macrophages with the liposomes decreased TNFα and nitric oxide (NO) secretion, while NAC increased the penetration of nanoparticles through the mucus. In vivo, we used LPS-induced lung inflammation model to assess the accumulation and therapeutic efficacy of the liposomes in C57BL/6 mice, either by intravenous (IV), endotracheal (ET) or IV plus ET nanoparticles administrations.

Using both administration methods, liposomes exhibited an increased accumulation profile in the inflamed lungs over 48 h. Interestingly, while IV-administrated liposomes distributed widely throughout the lung, ET liposomes were present in lungs parenchyma but were not detected at some distal regions of the lungs, possibly due to imperfect airflow regimes. Twenty hours after the different treatments, lungs were assessed for markers of inflammation. We found that the nanoparticle treatment had a superior therapeutic effect compared to free drugs in treating ARDS, reducing inflammation and TNFα, IL-6 and IL-1β cytokine secretion in bronchoalveolar lavage (BAL), and that the combined treatment, delivering nanoparticles IV and ET simultaneously, had the best outcome of all treatments. Interestingly, also the DPPC lipid component alone played a therapeutic role in reducing inflammatory markers in the lungs. Collectively, we show that therapeutic nanoparticles accumulate in inflamed lungs holding potential for treating lung disorders.

*Significance:* In this study we compare intravenous versus intratracheal delivery of nanoparticles for treating lung disorders, specifically, acute respiratory distress syndrome (ARDS). By co-loading two medications into lipid nanoparticles, we were able to reduce both inflammation and mucus secretion in the inflamed lungs. Both modes of delivery resulted in high nanoparticle accumulation in the lungs, intravenously administered nanoparticles

*Abbreviations:* ARDS, Acute respiratory distress syndrome; BAL, Bronchoalveolar lavage; CaAcOH, Calcium acetate; COPD, Chronic obstructive pulmonary disease; Dex, Dextrose; DLS, Dynamic light scattering; DMEM, Dulbecco's modified eagle medium; DPPC, 1,2-dimpalmiyristoyl-sn-glycero-3-phosphocholine; DPPE-Rhodamine, 1,2-dipalmitoyl-sn-glycero-3-phosphoethanolamine-N-(lissamine rhodamine B sulfonyl) (ammonium salt); ET, Endotracheal; EE, Encapsulation efficiencies; HPLC, High performance liquid chromatography; ICP, Inductively coupled plasma; IL-6, Interleukin-6; IV, Intravenous; IP, Intra peritoneum; IT, Intratracheal; Lip, Liposomes; LPS, Lipopolysaccharide; MPS, Methylprednisolone sodium succinate; NAC, N-acetylcysteine; NO, Nitric oxide; OD, Overdose; PEG2000, Polyethylene glycol 2000; TNF-α, Tumor necrosis factor alpha.

* Corresponding author.
*E-mail address:* avids@technion.ac.il (A. Schroeder).
[1] Contributed equally to this work

https://doi.org/10.1016/j.jconrel.2022.03.028
Received 1 October 2021; Received in revised form 10 March 2022; Accepted 15 March 2022
Available online 28 March 2022

reached lung endothelial while endotracheal delivery reached lung epithelial. Combining both delivery approaches simultaneously provided the best ARDS treatment outcome.

## 1. Introduction

Lung inflammation is characteristic in various respiratory diseases and injuries, such as asthma, chronic obstructive pulmonary disease (COPD), bronchiectasis, long COVID, and acute respiratory distress syndrome (ARDS) diagnosis [1].

ARDS is an inflammatory diffused form of lung injury that leads to increased pulmonary vascular permeability, resulting in secretion of interstitial fluids in the alveolar space and their collapse, making oxygen exchange difficult or impossible [2]. ARDS etiologies include, among others, severe trauma and sepsis, and a recent notable cause is SARS-CoV-2 infections (COVID-19) [3,4]. Patients with ARDS are severely hypoxemic, and existing therapy is mostly supportive but not curative, with mortality rates exceeding 40% [5]. Patients with ARDS tend to progress through three pathologic stages: the early exudative phase, the fibroproliferative phase, and the fibrotic phase. The lipopolysaccharide (LPS) insult model stimulates the exudative stage, which includes a nonspecific reaction to lung injury, interstitial edema, accompanied by acute and chronic inflammation [2,6,7].

Inflammation involves the activation of numerous immune cell types including neutrophils and macrophages [1,8,9]. While neutrophils perform extravasation towards the infected site to fight off invaders by degranulation and through phagocytotic behavior, pro-inflammatory macrophages produce cytokines such as TNF-α, IL-1β and IL-6 in response to bacterial components, such as LPS [10–13]. Moreover, in response to such stimuli, macrophages release reactive oxygen species (ROS) and produce nitric oxide (NO), which regulate inflammatory cells and protect the organism from potential dangers [14,15]. NO levels were used as an additional parameter for macrophage activation in vitro. The detection of cytokines in bronchoalveolar lavage (BAL) fluid is well corelated with the severity of inflammation in disease models, as verified by histological analyses [16].

Glucocorticoids, such as methylprednisolone (MPS) are used widely for treating lung inflammation [17–19]. Glucocorticoids diffuse through cell membranes leveraging amphipathic properties and cellular receptors. In the cytoplasm glucocorticoids bind glucocorticoid receptors reducing proinflammatory cytokine synthesis and inhibiting fibroblast proliferation and collagen synthesis via non-genomic and genomic pathways [20,21]. In addition, steroids decrease NO synthase in macrophages, leading to decreased NO secretion [22].

MPS was evaluated for treating early ARDS and showed positive therapeutic outcomes and improved survival [17,18] Methylprednisolone treatment of COVID-19 patients resulted in higher oxygenation index [19], with doses ranging from 1 mg/kg-body-weight per day to single doses of 40–500 mg [20]. However, systemic and prolonged administration of glucocorticoids is associated with severe side effects, such as interference with wound healing process, inhibition of effector cells in fighting active infections and other myopathic, cardiovascular and dermatologic side effects [23,24].

Additionally, a potential agent we tested for treating ARDS is *N*-acetyl cysteine (NAC) to treat mucus hypersecretion during inflammation that impairs blood-gas exchange. NAC is a mucolytic agent that reduces connecting disulfide bonds in mucus, thereby reducing mucus viscosity and accelerating mucus plugs removal [25–27]. Another therapeutic effect of NAC is as an antioxidant and decreasing the reactive oxygen species (ROS) [28,29]. A meta-analysis of ARDS patients that were treated with NAC found shorter hospitalization periods in the intensive care unit. Dose for NAC treatments varied from 40 to 210 mg/kg/day over 3–10 days [30] [31]. By oral administration, the bioavailability of NAC is less than 10% due to extensive first-pass metabolism [32].

The combination of NAC and corticosteroids was described in COPD patients, resulting in an improved oxidant burden [33]. Here, we tested an MPS and NAC combination in an ARDS model.

Drug concentrations at the target site following intravenous (IV) administration can be below the therapeutic window, therefore, to increase drug concentrations and bioavailability at the target site, decrease side effects, and prolonged the retention time of the drug at the target tissue we encapsulated drugs in 100-nm liposomes [34]. Specifically, we examined the effect of dipalmitoyl-phosphatidylcholine (DPPC) liposomes loaded with MPS and NAC on reducing lung inflammation, in the first stages of ARDS. Liposomal MPS uptake by macrophages and neutrophils can be mediated by adsorption, endocytosis, and phagocytosis [35], where drug release occurs intra- or extracellular.

The dipalmitoyl-phosphatidylcholine (DPPC) was chosen as the main component. DPPC is a naturally occurring pulmonary surfactant, that reduces surface tension at the air-liquid interface of the alveolus, thus preventing alveolar collapse associated with inflammation [36–38]. DPPC exerts its protective effect by integrating into plasma membrane of airway epithelium and immune cells affecting membrane integrity [38]. DPPC also acts as an immunomodulator by inhibiting cytokine release from innate immune cells in response to LPS [38].

Liposomes are already used in clinic for treating lung disorders and injuries [39–41]. For example, an Amikacin liposome inhalation suspension (ALIS) is used for treating pulmonary infections [42].

The proposed liposomal formulation was tested for its ability to reduce lung inflammation. Liposome's size was designed to be approximal 100 nm in order to improve penetration in inflamed tissues cite [43]. The study compared between endotracheal (ET) instillation to the lungs and intravenous (IV) administration, or both routes simultaneously. Previously, Garbuzenko et al. [44] compared the pharmacokinetics of approx.- 120 nm DOTA -based liposomes administered by IV and intratracheal. Results showed that liposomes administered intratracheally remained in the lungs for at least 72 h post-administration with low levels in other organs. However, liposomes administered by IV accumulated in lungs for the first hour and declined thereafter [44].

## 2. Materials and methods

### 2.1. Materials

DPPC (1,2-dimpalmiyristoyl-sn-glycero-3-phosphocholine), HSPC (hydrogenated soy phosphatidylcholine), DSPE-PEG2000 (1,2-distearoyl-sn-glycero-3-phosphoethanolamine-N-methoxy-polyethylene glycol 2000) were all purchased from Lipoid, Germany. was purchased from Biochempeg, USA. DPPE-Rhodamine (1,2-dipalmitoyl-sn-glycero-3-phosphoethanolamine-N-(lissamine rhodamine B sulfonyl) (ammonium salt)), cholesterol (57–88-5), *N*-acetylcysteine (NAC, 38520–57-9), Lipopolysaccharides (LPS) from *Escherichia coli* O26:B6 (L2762), D-(+) Glucose monohydrate (dextrose, 14,431–43-7), and mucin from porcine stomach (type II, 84082–64-4) were purchased Sigma-Aldrich. Methylprednisolone sodium succinate (MPS, solu-medrol) from Pfizer was used. Calcium Acetate was purchased from Spectrum.

### 2.2. Liposome composition process

Lipid mixture of DPPC, cholesterol and DSPE-PEG2000 was dissolved in absolute ethanol in 10% (*v*/v) solution volume and heated at 55°C. The lipid solution was added to calcium acetate solution. The liposomes were downsized using a Lipex extruder (Northern Lipids, Vancouver, Canada) five times through each 400, 200 and 100-nm polycarbonate membrane (Whatman, Newton, MA, USA) at 55°C with a maximal

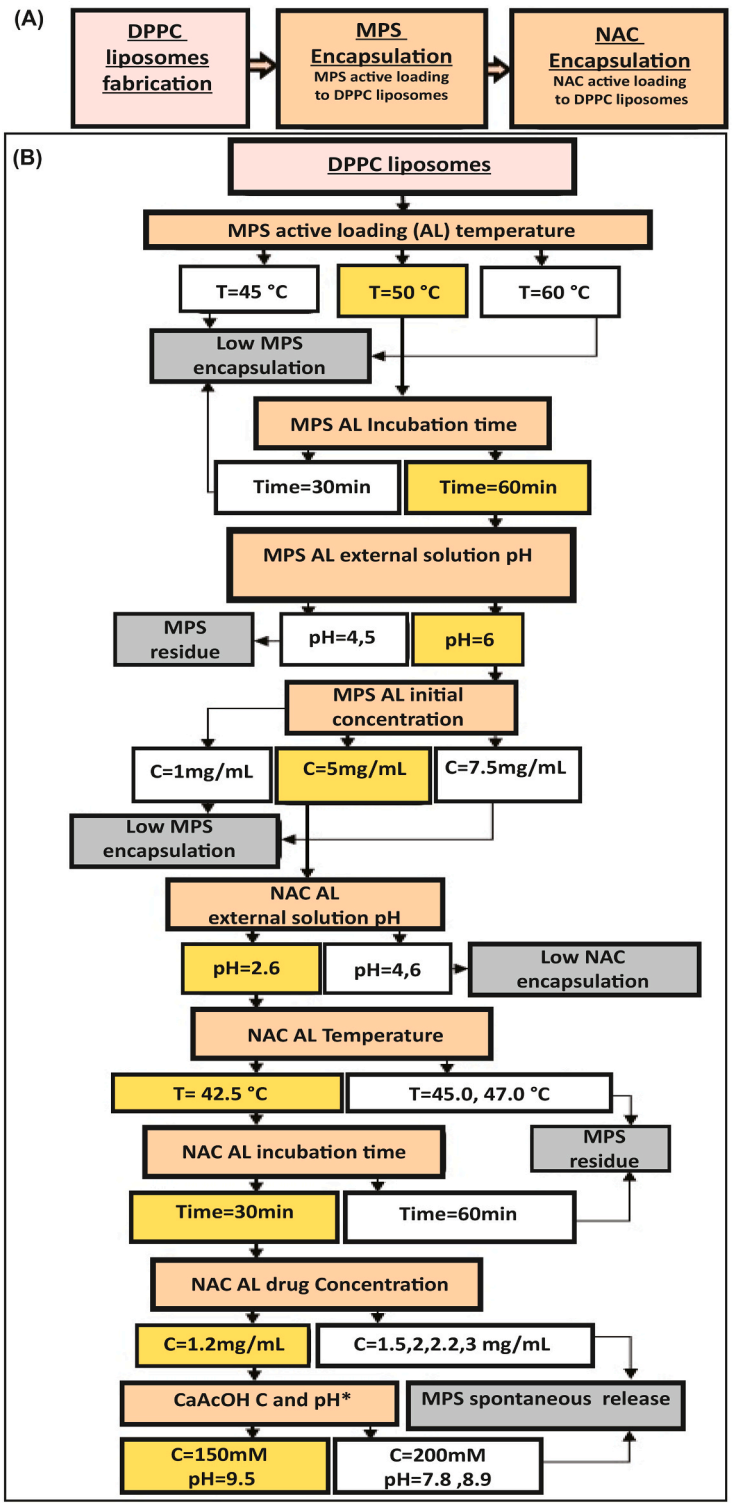


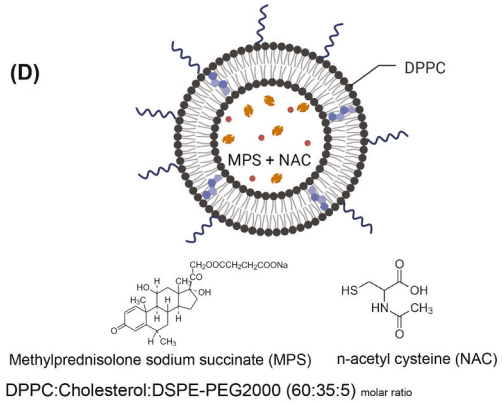


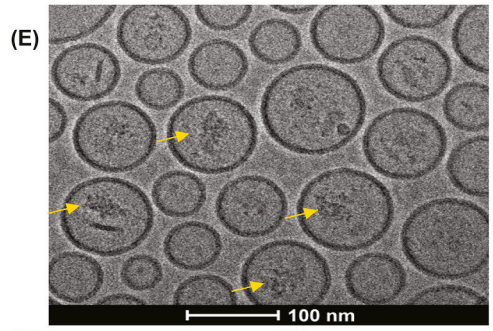


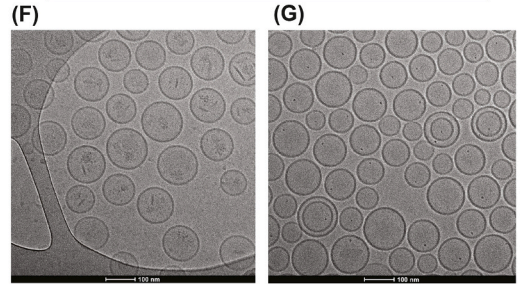


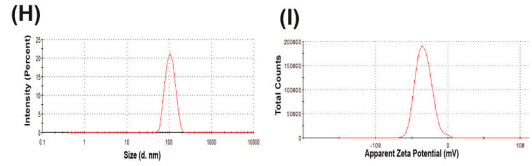


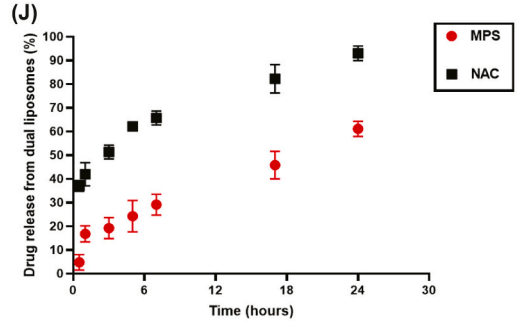


(C)

| CaAcOH (mM) | MPS initial (mg/mL) | MPS Temp (°C) | MPS Time (min) | NAC initial (mg/mL) | NAC Temp (°C) | NAC Time (min) | Final MPS C (mg/mL) | Final MPS EE (%) | Final NAC C (mg/mL) | Final NAC EE (%) | C (particle/mL) | Drug/lipid ratio (mol:mol) |
|---|---|---|---|---|---|---|---|---|---|---|---|---|
| 150 | 4.4 | 50 | 60 | 1.2 | 42.5 | 30 | 4.3 | 98 | 1.1 | 92 | 2.24E13 | MPS-7.2 NAC-5 |

(caption on next page)

**Fig. 1.** Physiochemical characterization of liposomes loaded with MPS and NAC. A) Liposomes loaded with two medicines (methylprednisolone (MPS), a steroid, and *N*-acetyl cysteine (NAC), a mucus active agent) were synthesized using a three-step formulation process. B) To reach high loading levels of both drugs and a stable formulation process we followed the following optimization methodology. Optimization steps varied drug concentrations, temperature, drug loading time, intra- and extra-liposomal pH, and the Active Loading (AL) salt concentrations. Selected conditions are labeled in yellow. Unfavorable outcomes are labeled in grey, and conditions leading to them in white. C) Summary table of final DPPC liposomal drugs formation process conditions and drugs' encapsulation analysis. (B—C) Drug and lipid concentrations were analyzed using HPLC-ELSD. Particle concentration and size were measured using dynamic light scattering (DLS). D) Schematic of DPPC liposomal drug formulation loaded with MPS and NAC. Formulation includes (dipalmitoyl-phosphatidylcholine) DPPC:cholesterol:DSPE-PEG2000 (1,2-distearoyl-sn-glycero-3-phosphoethanolamine-N-methoxy-polyethylene glycol-2000) (60:35:5 M ratio), with MPS and NAC encapsulated in the liposomal core. E) Cryo-TEM images of the MPS and NAC drug-loaded DPPC liposomes (scale bar = 100 nm), MPS liposomes (F) and NAC liposomes (G). H—I) Liposome size distribution and zeta potential measurement using DLS. J) In vitro Release of MPS and NAC from DPPC liposomes ($n = 3$). Active Loading (AL); Methylprednisolone succinate (MPS); *n*-acetyl cysteine (NAC). Fig. 1D was created using Biorender.com. (For interpretation of the references to colour in this figure legend, the reader is referred to the web version of this article.)

nitrogen pressure of 30 bar. The liposomes were dialyzed using a 12-14 kDa cutoff membrane (Spectrum Labs, CA, USA) against 4°C 5% dextrose solution (1:1000 vol. ratio). The external 5% Dextrose was replaced after 1, 4 and 24 h. After liposome were composed, liposomes were actively loaded with the drugs to compose the DPPC liposomal drugs (Fig. 1). First, MPS was encapsulated to the DPPC- liposomes by incubating 5 mg/mL MPS and liposomes at 50.0°C, 550 rpm shaking for 60 min at pH of 6.5. Then, NAC active loading was made by incubation of MPS liposomes with 1.2 mg/mL NAC at 42.5 °C, 550 rpm shaking for 30 min at pH = 2.6. After each encapsulation, dialysis was done to remove unencapsulated drugs. For fluorescently labeled liposomes 1% DPPE-Rhodamine or 0.3% DSPE-PEG2000-Cy3 or 0.3% DSPE-PEG2000-Cy5 were added to the lipid mixtures. For gadolinium (Gd)-liposomes, the lipid solution was added to 115 mg/mL DTPA-Gd dissolved in 5% dextrose. The non-encapsulated DTPA-Gd was removed by dialysis as well.

For mucus permeation experiment for Caco-2 cells, HSPC, cholesterol and DSPE-PEG2000 and DSPE-Cy7 (0.5%) liposomes were prepared and dialyzed as described above.

### 2.3. Liposome's characterization

Liposomal size and Zeta potential was measured using a Zetasizer Nano ZSP (Malvern Instruments, Worcestershire, UK) using appropriate polystyrene cuvettes after diluting the samples 1:100 in 5% dextrose. Liposome particle concentrations were measured using Zetasizer Ultra (Malvern, United Kingdom).

### 2.4. Drugs encapsulation

HPLC (High Performance Liquid Chromatography) was used for MPS, NAC and lipid detection (Agilent Technologies 1260 Infinity), applying reverse phase c18 column. Samples were diluted 1:10 in methanol. Buffers for MPS plan [45]: A-0.1% Acetic acid in water, HPLC grade, pH 5.2 (ammonium acetate) (MERCK, 1.01116.1000). B- Methanol, HPLC grade (MACRON, methyl alcohol anhydrous for HPLC, 6712–25), 4 mM ammonium acetate. Detection at wavelength 248 nm. Buffers for NAC [46]: A: 0.01 M octane-1-sulfonic acid sodium monohydrate, pH 2.2 adjusted with diluted phosphoric acid. B: mixture of 20% acetonitrile and 80% methanol. Detection at wavelength 200 and 214 nm. Final MPS and NAC concentrations were calculated using calibration curves.

Buffers for lipids (DPPC, Cholesterol and PEG 2000) plan: A-0.1% Acetic acid in water, HPLC grade, pH 5.2 (ammonium acetate) (MERCK, 1.01116.1000). B- Methanol, HPLC grade (MACRON, methyl alcohol anhydrous for HPLC, 6712–25), 4 mM ammonium acetate. Detection with ELSD.

### 2.5. CryoTEM liposomes image

Liposomes were imaged using Cryogenic transmission electron microscopy (Cryo-TEM). Cryo-TEM imaging was performed on a Thermo-Fisher Talos F200C, FEG-equipped high resolution-TEM, operated at 200 kV. Specimens were transferred into a Gatan 626.6 cryo-holder and equilibrated below −170 °C. Micrographs were recorded by a Thermo-Fisher Falcon III direct detector camera, at a 4 k × 4 k resolution. Specimens were examined in TEM nanoprobe mode using Volta phase plates for contrast enhancement. Imaging was performed at a low dose mode to minimize exposure of the imaged area to electrons. Images were acquired using the Tem Imaging and Acquisition (TIA) software. Liposomes diluted x20 with saline. Cryo-TEM specimens were prepared in a controlled environment vitrification system (CEVS) [47]. Since the system under study is aqueous, preparation was done in a temperature-controlled chamber with humidity at saturation, to prevent evaporation of volatiles [48]. Temperature was kept constant at 25 °C. A drop of the solution was placed on a carbon-coated perforated polymer film, supported on a 200 nm mesh TEM grid, mounted on tweezers. The drop was turned into a thin film (preferably less than 300 nm) by blotting away excess solution with a metal strip covered with a filter paper. The grid was then quickly plunged into liquid ethane at its freezing point (−183 °C). Prior to specimen preparation, grids were plasma etched in a PELCO EasiGlow glow-discharger (Ted Pella Inc., Redding, CA) to increase their hydrophilicity.

### 2.6. In vitro release rate of NAC and MPS

NAC and MPS release profiles from liposomes were measured by dialysis of the samples (free or DPPC liposomal drugs) against 5% dextrose at a 1:750 volume ratio, 37 °C and 50 rpm shaking, using 12-14 kDa cutoff membrane (SpectraPor). Drug concentrations were measured using HPLC.

### 2.7. Cell culture

Raw 264.7 macrophage line was purchased from ATCC. The macrophage cells were grown in DMEM medium, with 10% FCS and 1% penicillin-streptomycin, 0.5% Amphotericin B. Macrophages were cultured in 24-well plates at a concentration of $0.5*10^6$cells/well and grown at 37 °C, 5% $CO_2$. 15 h later, cells were stimulated with 0.5 mL 1000 ng/mL LPS [49] to induce activation. 2 h later, LPS was removed, and cells were treated with MPS liposomes, NAC liposomes, both NAC and MPS liposomes encapsulated (DPPC Liposomal drugs), free NAC, free MPS, free NAC and MPS mix, 5% dextrose and DPPC liposomes. It must be mentioned that all liposomes and drugs were dissolved in 5% dextrose solution, and hence all treatments were compared to 5% dextrose solution. 100 μL of each treatment was added to 400 μL medium. 2 h later, treatment was removed, and fresh medium was added. 24 h from LPS induction, medium was collected. Medium was examined for nitric oxide (NO) and TNFα levels using Griess reagent and ELISA, respectively.

### 2.8. NAC effect on liposome-mucus penetration

To examine liposomes infiltration to the mucus, mucus and Cy5-labeled liposomes were imaged under confocal microscopy, with and without NAC treatment. Mucin from the porcine stomach was dissolved

to a concentration of 43.75 mg/mL in PBS and gently shaken overnight in RT to form a disulfide bond and form mucus. The mixture was let to achieve relaxation for 24 h. 10 mg/mL NAC was dissolved in PBS for NAC treatment. 8 μL of synthetic mucus was dripped on microscope slide. 2 μL of 10 mg/mL NAC treatment was dripped on top. After 1 h of incubation, 2 μL liposome were placed on top of the described set. A coverslip was placed on top with spacers that ensured that the coverslip was evenly spaced. PBS solution used as control. Images were taken using Zeiss LSM 700 Confocal laser scanning microscopy, and were processed using Zen 3.4 Blue edition.

### 2.9. Mucus and NAC effect on cells liposomes uptake

To examine in-vitro cells uptake efficiency under mucosal conditions, we developed an in-vitro mucus permeation assay using human colorectal adenocarcinoma Caco2 cell line. These cells are naturally covered with mucus layer in the intestine and therefore act as a good model for this purpose. Mucin from the porcine stomach was dissolved to a concentration of 10 mg/mL in PBS and gently shaken overnight in RT to form a disulfide bond and form mucus. The cells were cultured separately in 24-well plates for 5 days, with fresh medium replacement after 3 days, with RPMI medium. Then, the cells were covered with 200 μL of mucus to create a uniform layer on top of the cells. Since NAC breaks S—S bonds, it breaks the mucus structure. We also compared the uptake with 0.7 mM concentration of NAC treatment and examined the improvement in liposomes cells uptake. Following mucus settlement on the cells, liposomes labeled with Cy7 were added to each well in 10% volume with the medium and incubated in 37 °C, 5% $CO_2$ with and without the NAC treatment. After 2 h, the mucus and medium were removed, and the cells were washed twice with PBS. DAPI was added in 1:1000%*v*/v with fresh PBS and fixed using 4% paraformaldehyde (PFA). The cells were imaged using x10 magnification with Lionheart FX automated microscope (BioTek). Cells uptake was quantified by nuclei and liposomes fluorescence labling using Gen5 Image Prime software (ver. 3.10, BioTek).

### 2.10. Animal model - LPS induced lung inflammation in mice

Mice were anesthetized with ketamine 80 mg/g BW, xylazine 4.5 mg/g BW and buprenorphine 100 mg/g BW, intra peritoneum (ip). 20 g catheter insert endotracheal (ET). To confirm tube's presence in the trachea, 60 μL saline was aspirated into a syringe. The syringe was then connected to the catheter, and if the tube was in the right place, the saline bubble moved at the rate of mice breathing. LPS from *E. coli* O26: B6 was dissolved in saline to concentration of 5 mg/mL. 20 μL LPS was given ET in 2 doses (with a 5 min interruption) to C57BL/6 anesthetized male mice. Lung inflammation in mice was analyzed by TNFα, IL-1α and IL-1β and IL-6, cytokines levels in BAL fluid and histology slides as described in Fig. 5. The experiments described here were approved by the ethics committee (Ethical request No. IL-0470518 and IL-1020820).

### 2.11. Biodistribution in vivo

Rhodamine-labeled and Gd-DTPA loaded liposomes, in the same composition as the drug encapsulated liposomes, were composed and were administered to mice intravenously (IV), endotracheally (ET) 6 h after LPS exposure. After different time points (1, 3, 6, 12, 24 and 48 h) mice were euthanized by ketamine-xylazine overdose (OD) and organs were extracted and have been weighed. Organ samples were imaged ex vivo via IVIS Spectrum CT Pre-clinical in-vivo imaging system (PerkinElmer, MA, USA). Then, organs were heated to 500 °C for 5 h and their ashes were dissolved in 1% nitric acid (*v*/v) (Bio Labs, Israel). Gd concentration of each sample was measured using a standard calibration curve at the range of 0.01–50 ppm. Gd was quantified using Inductively Coupled Plasma - Optical Emission Spectroscopy (ICP-OES, 5100-Agilent).

### 2.12. Cryosection for liposomes distribution in the lung

Lung inflammation induced in mice. After 6 h, 20 μL Cy3-liposomes were ET administered and 200 μL Cy5-liposomes were IV injected. One hour after liposome administration, mice were euthanized by ketamine-xylazine overdose OD. 200 μL of optimal cutting temperature (OCT) (Scigen, Tissue-Plus) diluted with PBS 1:1 (*v*/v) was injected into lungs via trachea, and lungs were extracted. Lungs were frozen using liquid nitrogen steam. Lungs were cut into 10 μm thickness samples using cryostat (Leica CM1950, Germany). Lungs were mounted with DAPI Fluoromount-G (SouthernBiotech, CAT 0100–20). Leica DMI8 inverted fluorescent microscope and Confocal710 microscope were employed to examine liposome distribution in the lungs via two different administration pathways. Acquisition was performed using the LAS-X and ZEN software, respectively.

### 2.13. In vivo efficacy

6 h after inflammation induction (LPS ET 5 mg/mL, 20 μL per mouse) treatment were administered by IV (200 μL), ET (20 μL) or both IV and ET. The lower amount delivered ET was intended to prevent suffocation due to increased edema associated with lung inflammation treatments were DPPC liposomes, free drugs or DPPC liposomal drugs. Drug's concentrations were 4.3 mg/mL and 1.1 mg/mL for MPS and NAC, respectively. 26 h after inflammation induction mice were sacrificed, and inflammation was characterized based on lung tissue histological staining (H&E) and cytokines in BAL fluid.

### 2.14. Lung histology

Mice were euthanized. 100 μL of 4% natural buffer formalin (NBF) (Sigma-Aldrich) was injected into lungs via trachea. Lungs were extracted and kept in 4% NBF. Slides were cut and hematoxylin and eosin (H&E) staining was performed using Patho-Lab service. Slides were scanned using automatic slide scanner 250 flash.

### 2.15. Bronchoalveolar lavage (BAL) fluid

Mice were euthanized by ketamine-xylazine OD and 22 g catheter was inserted into mouse's trachea. 700 μL of cold PBS was injected into the lungs. The lungs were gently massaged and after 30 s the fluid was sucked out from the lungs and kept at 4 °C until cytokine analysis.

### 2.16. Cytokine identification

Cytokines were identified in BAL fluid supernatant or in macrophage medium to evaluate immune cell response. ELISA was carried out using PeproTech kit (900-K54, 900-K50, 900 M-47, 900-K00, PeproTech Asia) protocol.

## 3. Results and discussion

### 3.1. MPS, NAC and DPPC liposomes

Liposomes were composed of DPPC, cholesterol and DSPE-PEG2000 [50,51] at molar ratio of (60:35:5), respectively. DPPC and cholesterol were selected since they are a naturally occurring components of the pulmonary surfactant [52] (Fig. 1D). DPPC Liposomes were loaded with both MPS and NAC, using active remote (active) loading approach [53]. For this, DPPC liposomes (102.6 ± 0.3 nm, PDI = 0.06, zeta potential = −34 ± 10 mV, Fig. 1H–I) were loaded with calcium acetate (CaAcOH, 150 mM) as an osmotic pump. Drugs were actively loaded one after that other: MPS first, followed by NAC loading (Fig. 1A). For each drug encapsulation process, different loading conditions, such as pH, drug concentration, temperature and time of incubation were examined, as detailed in Fig. 1B.

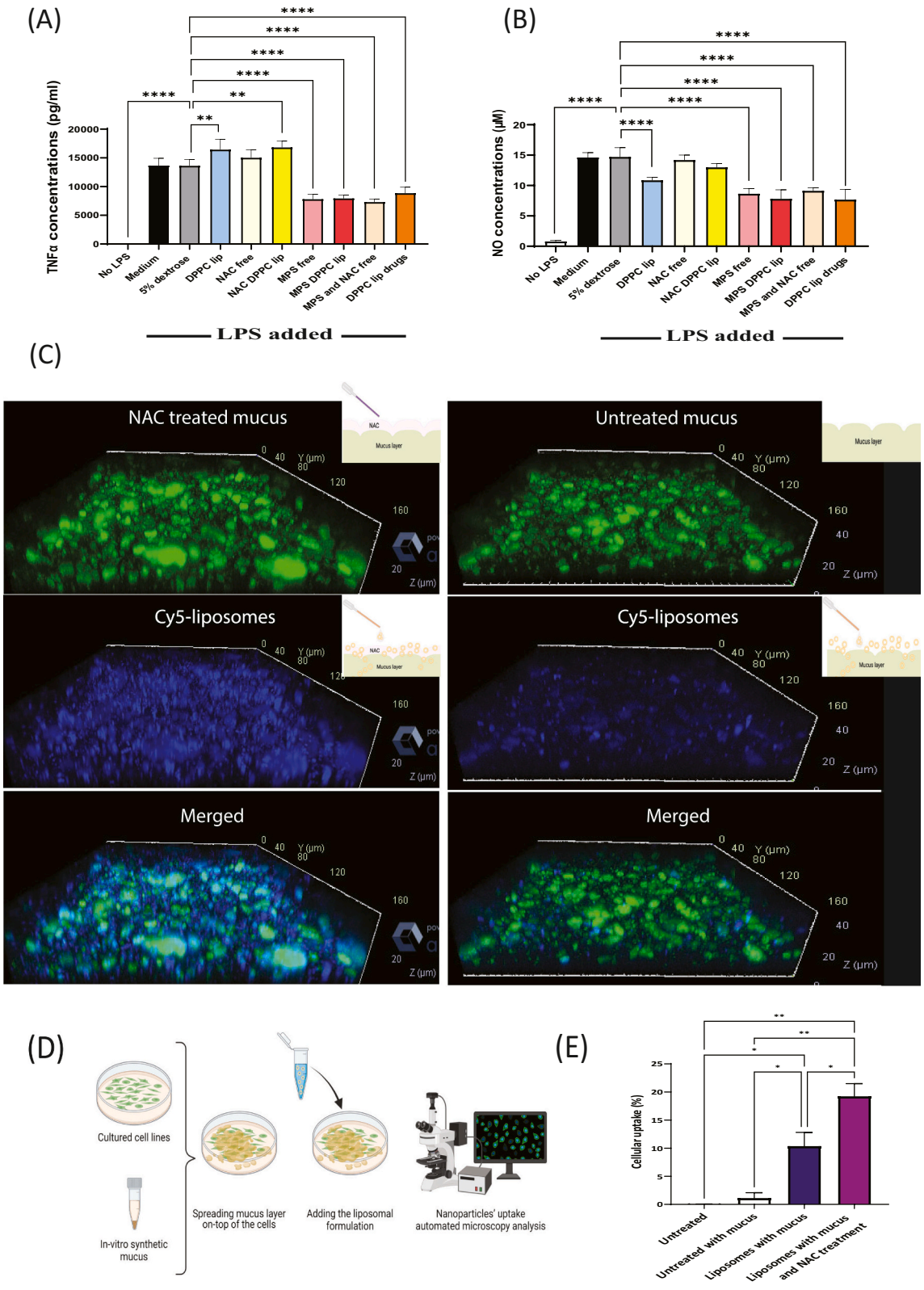


**Fig. 2.** NAC increases mucus permeability and MPS reduces macrophage cytokine secretion.
A-B) Measuring of LPS-induced macrophage cytokine (TNFα and nitric oxide (NO)) levels following liposomes treatments. One-way ANOVA and one-tailed *t*-test were performed using PRISM: $^{*}P < 0.05$, $^{**}P < 0.01$, $^{***}P < 0.001$. Asterisk above bars connecting columns represents a significant difference between groups. C) Confocal images of 100 nm liposomes of NAC treated, or untreated, mucus's penetration. D) In-vitro mucosal barrier permeation assay – cells were plated on 24 walls petri dish and a layer of 200 μL synthetic mucus was applied on top of the cells as a biological barrier. The ability of nanoparticles to cross the mucus layer and be taken up by the underlying cells was quantified over time using an automated microscope setup. E) Automated microscopy images of Caco-2 cellular uptake of Cy-7 fluorescently labeled 100 nm liposomes. The uptake is presented as mean ± SD. One-way ANOVA with an adjusted *P*-value of multiple comparisons tests was used for statistical analysis; $^{**}P < 0.01$; $^{*}P < 0.05$. Fig. 2c and 2D was created using Biorender.com.

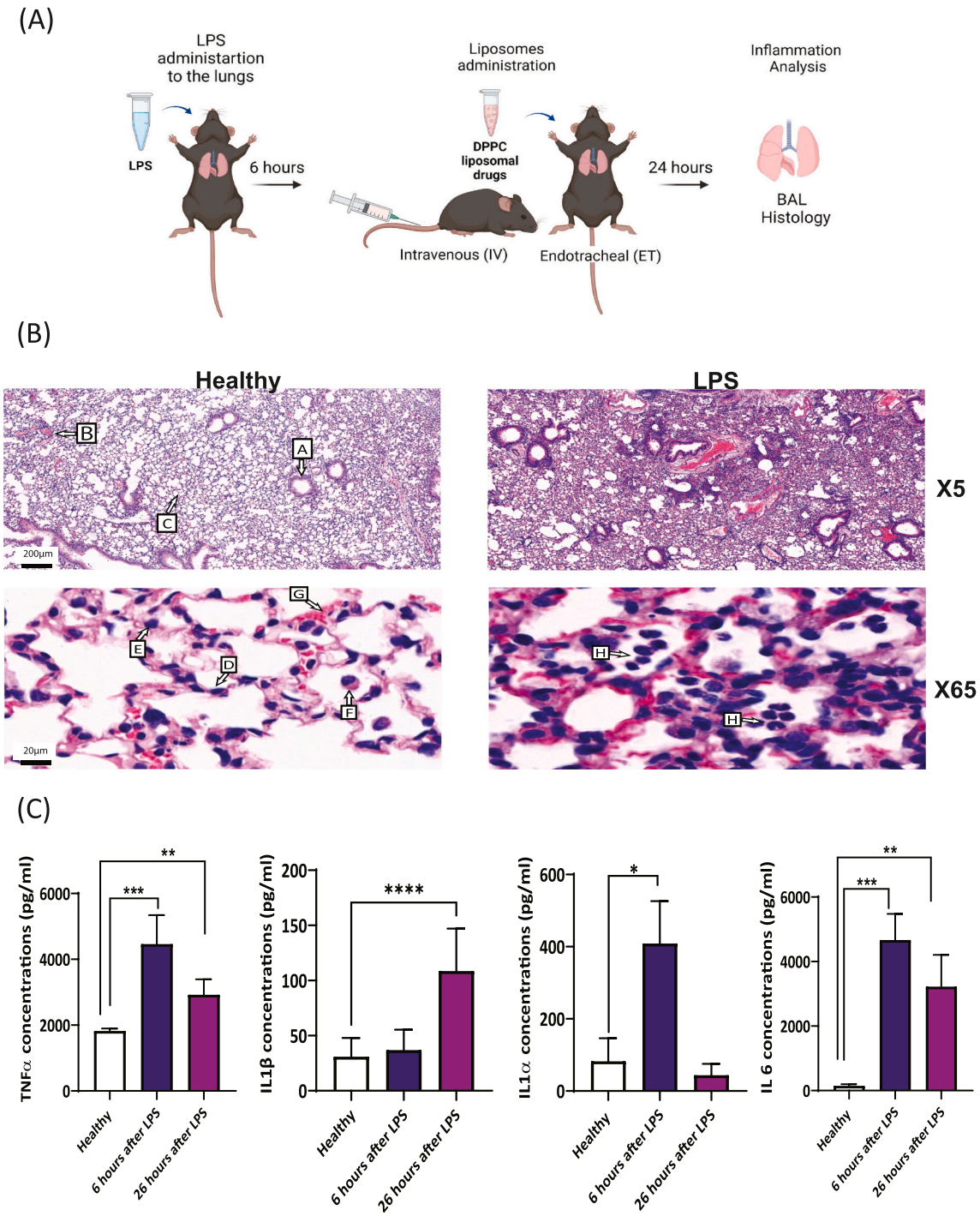


**Fig. 3.** In vivo lung inflammation model.
A) LPS is administrated endotracheally to induce inflammation. Six hours later, intravenous (IV) or endotracheal (ET) or both IV plus ET treatments were initiated. B) H&E staining of healthy and inflamed lungs 24 h after LPS administration: Arrows indicate, A- distal airway, B- blood vessel, C- alveolar ducts, D- type 1 pneumocytes epithelial cells; *E*- type 2 pneumocytes epithelial cells, F- alveolar macrophages, G-endothelial blood vessel cell. H- neutrophils and macrophages within airspaces (scale bar = 200 µm and in zoom-in image scale bar is 20 µm) C) Analysis of Inflammatory markers kinetics. TNFα, IL1α, IL1β and IL6, levels in BAL fluid were quantified using ELISA assay. Healthy mice ($n = 1$), LPS mice ($n = 3$), Dunnett's multiple comparison test $^{**}P < 0.01$; $^{**}P < 0.001$; $^{***}P < 0.0001$. Asterisk above bars connecting column represents significant difference between groups. Fig. 3A was created using Biorender.com.

Drug concentrations in the liposomes reached 4.3 mg/mL and 1.1 mg/mL for MPS and NAC, accordingly, with encapsulation efficiencies of 98% and 92% (%EE). Drug-to-lipid molar ratios are 7.2 and 5 for MPS and NAC, respectively. DPPC liposomal drugs particles concentration was $2.24*10^{13}$ particle/mL, as summarized in Fig. 1C.

In addition to drug encapsulation concentration, liposomes were tested for their stability and drug release profiles under physiological conditions: 50% of encapsulated NAC and 20% of the MPS released over 3 h, increasing to 60% for NAC and 90% for MPS release after 24 h (Fig. 1J). Cryo-TEM imaging of the liposomes indicated spherical vesicles with MPS and NAC, with what seems like drug precipitation in the intraliposomal aqueous core (Fig. 1E). In addition MPS liposomes (F) or NAC liposomes(Fig. 1G) were imaged.

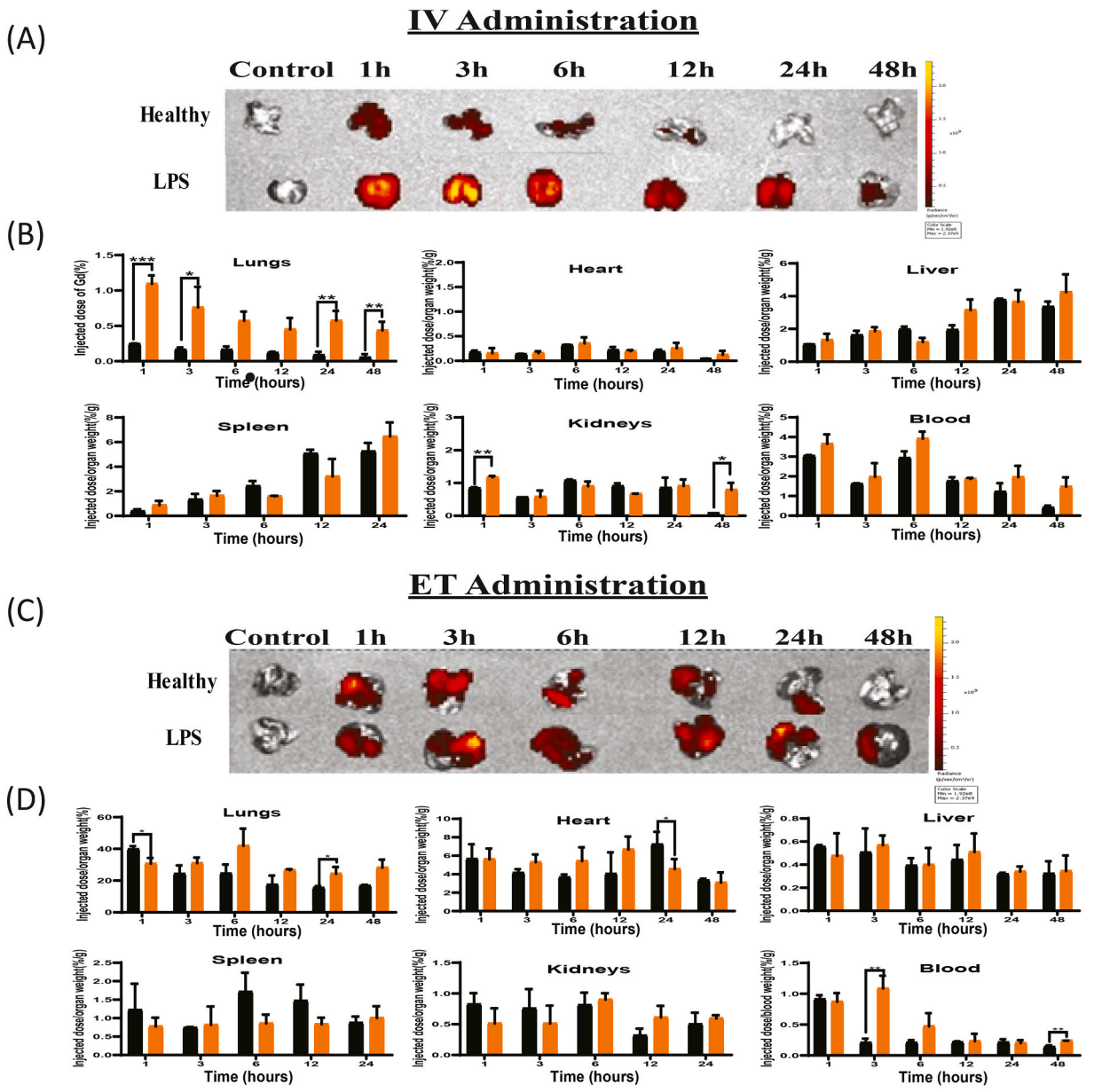


*(caption on next page)*

**Fig. 4.** Biodistribution of liposomes in inflamed lung.
A) Ex-vivo representative images of healthy and inflamed lungs at varying time points after IV injection of rhodamine and Gd labeled liposomes taken by whole animal IVIS imaging system. B) Biodistribution of rhodamine and Gd labeled liposomes at different time points from IV injection as measured using elemental analysis (ICP-OES) of the lungs, heart, liver, spleen, kidneys and blood. C) Ex-vivo representative IVIS images of lungs at varying time points after ET administration of rhodamine and Gd-labeled liposomes. D) Biodistribution rhodamine and Gd labeled liposomes at different time points from ET administration as measured by ICP-OES in lungs, heart, liver, spleen, kidneys and blood. Healthy mice ($n = 4$), LPS mice ($n = 3$). One way ANOVA and one tailed *t*-test were performed using PRISM: $^{*}P < 0.05$, $^{**}P < 0.01$, $^{***}P < 0.001$. Asterisk above bars connecting columns represents a significant difference between groups. E) Confocal images of inflamed lung cryo-sections following Cy3-labeled liposomes administered via ET alongside Cy5-labeled liposomes administrated IV. Nuclei were stained using DAPI. Arrows exhibit high intensity of liposomes present. Arrowheads show liposomes in a blood vessel and arrows show liposomes in the airway. Scale bar = 200 μm.

### 3.2. Treating activated macrophages cell line

We examined the effect of DPPC liposomal drugs on RAW264.7 macrophages after beginning exposed to LPS. TNFα levels and Nitric oxide (NO) decreased significantly following treatment with DPPC liposomal drugs, MPS liposomes, free MPS plus NAC mix, and free MPS, in comparison to untreated LPS induced cells (Fig. 2A–B). Comparing the free drug versus the liposomal treatment demonstrates benefit or equal therapeutic influence. Interestingly, empty DPPC liposomes showed ~25% NO decrease which may be attributed to the anti-inflammatory nature of the lipid [37,38,54] (Fig. 2A–B).

### 3.3. Effect of NAC on liposomes penetration in vitro

We examined the effect of NAC on liposomal mucus penetration. NAC treatments improved liposomes mucus penetration in comparison to untreated mucus (Fig. 2C). The NAC, agent with thiol-amino structures which gives it the mucolytic feature, disrupts the disulfide bonds in the mucus [55].

### 3.4. Effect of NAC on cellular uptake under mucosal conditions in vitro

To examine the effect of NAC treatment on liposomes cells uptake under mucosal conditions, we developed an in-vitro mucus permeation assay by spreading a mucus layer over Caco2 cells followed by automated imaging of the liposomal uptake by the cells undernieth the mucus [56] (Fig. 2D). The addition of NAC improved nanoparticle uptake by 1.8-fold, compared to cells with mucus without NAC treatment (Fig. 2E).

The NAC dissolves the disulfide bonds of the mucus, has previously been used to remove the secreted mucus layer from cell cultures without cellular damagev [57,58].

### 3.5. Acute inflammation model

Acute lung inflammation was induced via ET LPS administration as described schematically in Fig. 3A [59,60]. Blinded pathologic assessment of mice lungs examined the inflammatory state of the lungs (Fig. 3B). Compared to healthy lungs, LPS induced lungs had acute inflammatory infiltration with neutrophils filling the alveolar space. Vascular congestion and extravasated RBCs were also seen.

Furthermore, cytokines in BAL fluid were analyzed 6 and 26 h after LPS induction (Fig. 3C). IL-1α, TNF-α and IL-6 cytokine concentrations were significantly higher compared to healthy control after 6 h (TNFα: $P < 0.001$, IL1α: $P < 0.01$, and IL6: $P < 0.001$), while, at 26 h, TNF-α, IL-1β, and IL-6 levels were higher compared to healthy control ($P < 0.01$, $P < 0.0001$, $P < 0.01$, respectively), together demonstrating acute inflammation and criteria for ARDS.

### 3.6. IV versus ET nanoparticle' biodistribution in mice

#### 3.6.1. Biodistribution kinetics of IV-injected liposomes

We tested the liposomal biodistribution to different organs at different time points (1,3,6,12,24, and 48 h post IV-injection) in healthy and acute LPS lung inflamed mice. Whole-animal IVIS imaging demonstrates increased liposomal accumulation in the inflamed lungs compared to the healthy. One hour after liposomal IV administration, Rhodamine-labeled liposomes accumulated in LPS-induced lungs at 2.5-fold higher levels than in the healthy lungs. This higher accumulation in inflamed tissues may occur due to increased vascular permeability at sites of inflammation as well [61,62] as increased mononuclear phagocytes system internalization of liposomes at inflammatory sites. This trend of higher accumulation of liposomes in LPS-induced mice was observed at all time points (Fig. 4A, Sup. C) reaching up to 8-fold increase at 48 h (Fig Sup. A). The enhanced accumulation of liposomes in inflamed lungs indicate a key potential of liposomes to target ARDS.

To quantify the biodistribution of liposomes, Gadolinium (Gd)-loaded liposomes were administered either IV or ET and Gd content was assessed in the different organs using ICP-OES elemental analysis. Gd content in heart, liver, spleen, kidneys, and blood are displayed as injected-dose-per-organ-weight (%/g) at varying time points, Fig. 4B. Gd content in lungs was normalized to the initial injected dose due to the apparent pulmonary edema observed in inflamed lungs which can alter weight measurements. In lungs, a Gd concentration of $1.09 \pm 0.09\%$ was observed 1-h after administration, compared to $0.240 \pm 0.005\%$ in healthy lungs. Moreover, a significant increase in Gd content in the healthy versus inflamed lungs was recorded 4 and 48 h after the administration (6.5 and 8-fold-increase respectively). The Gd content in the heart, liver, spleen, kidneys, and blood was similar. In conclusion, both qualitative (IVIS) and quantitative (ICP-OES) analysis demonstrate the increased accumulation of liposomes in inflamed lungs.

Both Rhodamine and Gd analysis exhibited a similar clearance profile (Fig. 4A–B). Liposomes were present in inflamed lungs even 48 h post-injection, compared to 12 h in healthy lungs (Fig. 4A–B).

#### 3.6.2. Kinetic biodistribution of ET administered liposomes

The biodistribution of liposomes administered by endotracheal intubation (ET) was assessed. IVIS images demonstrate the liposomes presence in the lungs at varying time points, in healthy and LPS-induced mice after endotracheal administration (Fig. 4C, Sup. B—C). One hour after administration, both Rhodamine and Gd analysis showed somewhat higher accumulation in healthy lungs compared to the inflamed lungs, however, thereafter the accumulation of the nanoparticles in the inflamed lung was greater (Fig. 4C–D, Sup. A-B). We propose that mucus accumulation and breathing impairment among the LPS induced mice, led to reduced absorbance of the particles from the trachea. Six-hours post ET administration, healthy mice show a decrease in liposome accumulation compared to LPS-induced mice. The fluorescent signal in inflamed lungs after 12 h is $(4.03 \times 10^8 \pm 0.49 \times 10^8$ p/s/cm$^2$/sr) in LPS-induced mice compared to $(9.29 \times 10^7 \pm 0.63 \times 10^7$ p/s/cm$^2$/sr) in healthy mice. To examine the liposomal accumulation in lungs, heart, liver, spleen, kidneys, and blood, quantitative Gd measurements were performed using ICP-OES (Fig. 4D). Six, 12, 24 and 48 h after endotracheal administration, inflamed lungs showed higher Gd concentrations (1.7,1.5,1.5,1.7 fold-increase respectively) compared to the healthy lungs. In other organs, there was no significant difference in Gd concentration at all time points (Fig. 4D).

In conclusion, administration of liposomes through ET shows higher retention rates in inflamed lungs compared to IV administration at all time points. Furthermore, the accumulation of liposomes is higher in inflamed versus healthy lungs.

Lung inflammation is orchestrated by elevated cytokine levels in the

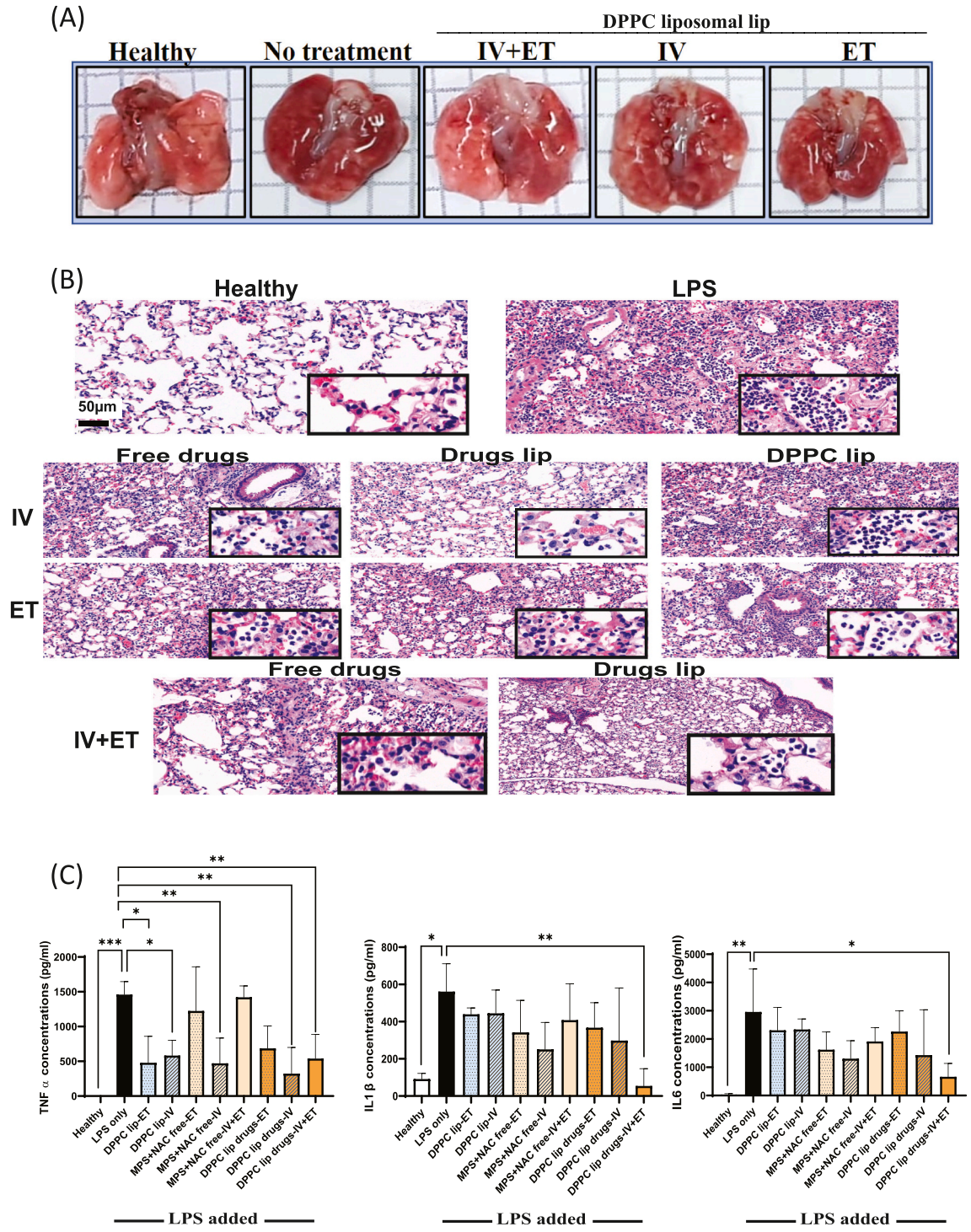


**Fig. 5.** Efficacy experiments of the DPPC liposomal drug delivered ET, IV or both.
A) Representative images of healthy lungs, untreated inflamed lungs, and inflamed lungs after IV plus ET, IV and ET treatment of DPPC liposomal drugs. B) H&E sections of lungs treated IV, ET or IV plus ET, with free drugs, empty DPPC liposomes or drug loaded DPPC liposomes. Scale bar 50 μm (X23). Square shows magnification of X150 exhibiting infiltration of lymphocytes into alveoli. C) Levels of bronchoalveolar lavage (BAL) fluid pro-inflammatory cytokines were quantified after different treatments (ET, IV and IV + ET), TNFα, IL1β, and IL-6 levels in the BAL fluid. One-way ANOVA and one-tailed *t*-test were performed using PRISM: $*P < 0.05$, $**P < 0.01$, $***P < 0.001$. The asterisk above bars connecting columns represents a significant difference between groups.

blood secreted by multiple sites in the body. IV DPPC liposomal drugs have been shown to target multiple inflammatory sites simultaneously [43] (for example the liver). Overall, the liposomal treatment decreased systemic cytokines levels in the lung and reduced the secretion of chemical mediators that induce inflammation.

### *3.6.3. Simultaneously administered IV and ET liposome biodistribution in inflamed lung*

We imaged the targeting of lung parenchyma from both the epithelium (by ET administration), and endothelial side of the blood vessel cells (via IV administration), 1 h after liposomes administration to inflamed lung (Fig. 4E). Liposome administrated via IV were widely

present throughout the lung, taking advantage of the spread capillary net in the lungs (Cy5 liposomes, red). In addition, high liposomal accumulation was observed in the endothelial blood vessels (Fig. 4E, arrowhead). Liposomes administrated endotracheally, were widely present in lungs with higher intensity (Cy3 liposomes, green) compared to IV administered liposomes. However, via ET administration some distal regions of the lungs, did not have liposomal presence, possibly due to impaired ventilation to these sites in inflamed lung with spontaneous breathing. High liposomal accumulation was observed in the epithelial airway (Fig. 4E, arrows).

### 3.7. DPPC liposomes improve in vivo efficacy

DPPC Liposomal drugs were administered to mice 6 h after LPS induction (LPS ET 5 mg/mL, 20 μL per mouse), treatments were administered IV (200 μL), ET (20 μL) or both IV and ET. The lower volume delivered ET was intended to prevent suffocation. 26 h after LPS induce, the mice were sacrificed, and inflammation was characterized by histological staining (H&E) and cytokine analysis in the BAL fluid (TNF-α and IL-6). The nanoparticle treatments reduced inflammation in the lungs, suggesting a positive effect for combined treatment (Fig. 5A).

Histologic sections were blindly analyzed demonstrating that the untreated group present a severe acute inflammatory reaction with neutrophils filling alveolar spaces. Lungs obtained from mice treated by DPPC liposomal drugs via IV or IV and ET, showed very mild to mild inflammatory infiltration. Lungs treated with the free drug IV or ET plus IV, showed a mild inflammatory reaction. Interestingly, intravenous administration of either free drugs or DPPC liposomal drugs resulted with milder inflammatory infiltrate compared to ET administration (Fig. 5B). The percent of severe inflammation in the alveoli relative to the total lung were analyzed histopathologically to quantify the lungs injury, demonstrating that treatment with DPPC liposomal drugs was superior in reducing lung severity (Sup. D).

To further establish the effect of the liposomal treatment, we determined the levels of TNF-α, IL-1β and IL-6 cytokines in the BAL fluid. Levels of IL-6 significantly decreased following combined IV and ET treatment compared to the untreated mice (664 pg/mL and 2962 pg/mL respectively, Fig. 5C). No significant decrease in cytokine levels was observed 26 h after free ET or combined ET plus IV administration of drugs treatment. The levels of TNF-α significantly decreased following DPPC liposomes, liposomal drugs IV and IV plus ET administrations (322 pg/mL and 540 pg/mL respectively) when compared to untreated inflamed mice (1459 pg/mL), or to mice receiving free drugs (Fig. 5C). Similarly, the levels of tested IL-1β were the lowest in mice that received ET plus IV treatment routes (5-fold decrease) compared to other routes.

In conclusion, while reduction in inflammation markers (TNF-α, IL-1β and IL-6) was recorded after all treatment modalities, highest reduction was observed in the combined ET plus IV administration.

## 4. Conclusions

In this study, we developed DPPC liposomes co-loaded with the corticosteroid MPS, and the mucus active agent NAC into liposome through sequential drug loading to treat ARDS in vivo, as a model of acute lung disease.

Following systemic IV administrations, liposome accumulation was more significant in inflamed lungs in comparison to healthy lungs, indicating that liposomes exhibit preferential targeting of the inflamed lung. Local administration of liposomes via the ET route leads to a greater amount and longer retention time of liposomes in inflamed lungs.

An additional significant difference between IV and ET routes is that IV administered liposome distribution spanned across the whole lung, while ET liposomes were distributed mostly in lung parenchyma but were not found at partial distal areas of the lung.

Therefore, combining ET and IV administration modes stimulates lung accumulation in the lungs from both alveolar epithelial and endothelial blood vessel cells, allowing broad coverage of lungs.

Both in vitro free drug and liposomal treatments of Lps-stimuli macrophages showed an analogous trend for TNF-α, and NO levels decreased. It can be concluded that DPPC liposomal drugs availability is significant since effect is seen.

The in vivo experiment demonstrated the best outcomes for IV plus ET administrations of DPPC liposomal drugs, explained by the improved lung coverage.

DPPC liposomes decreased NO levels in vitro, and TNFα levels in vivo, demonstrating some therapeutic effect of the lipid component alone.

The DPPC liposomal system is a promising platform for treating lung diseases.

## Authors Credit

A. Schroeder conceived the approach, supervised, and directed the research. S. Arber Raviv and M. Alyan contributed equally to this work. S. Arber Raviv, M. Alyan, H. Korach-Rechtman, L. Koren, J. Shainsky, J. Shklover, designed the experiments. S. Arber Raviv, M. Alyan, E. Egorov, A. Zano, M. Yaskin Harush, A. Saadya, O. Doppelt Flikshtain, L. N. Mekies, and L. Koren performed the experiments. S. Arber Raviv, M. Alyan, H. Korach-Rechtman, S. Farkash, O. Doppelt Flikshtain, and L. Koren analyzed the data. G. Kaneti, I. Nudelman, Y. Gal, E. Dor, and Y. Adir contributed to experimental design. J. Shklover and J. Shainsky managed and coordinated the research. All authors contributed to data analysis and preparation of the manuscript.

## Conflicts of interest

The authors declare no conflict of interest.

## Acknowledgements

This project has received funding from the Ministry of Defense, European Union's Horizon 2020 research and innovation program under grant agreement No 680242-ERC-[Next-Generation Personalized Diagnostic Nanotechnologies for Predicting Response to Cancer Medicine]; the Israel Science Foundation (1421/17); The Israel Ministry of Science & Technology (3-16963, 3-17418); the Phospholipid Research Center Grant (ASC-2018-062/1-1); Leventhal 2020 COVID19 Research Fund (ATS #11947); The Israel Ministry of Economy for a Kamin Grant (52752, 69230); Ministry of Agriculture & Rural Development - Office of the Chief Scientist (323/19); Israel Innovation Authority for Nofar Grant (67967); the German-Israeli Foundation for Scientific Research and Development for a GIF Young grant (I-2328-1139.10/2012); the European Union FP-7 IRG Program for a Career Integration Grant (908049).

Greatly appreciated support of the Louis family Cancer Research Fund; a Mallat Family Foundation Grant; The Unger Family Fund; a Carrie Rosenblatt Cancer Research Fund, A. Schroeder also acknowledges Alon and Taub Fellowships. The authors also acknowledge the support of the Russell Berrie Nanotechnology Institute, the Technion Integrated Cancer Center (TICC) and the Lorry I. Efrat Barak, Yousef Mansour, Nitzan Dahan, Yael Lupu-Haber from Lokey Interdisciplinary Center for Life Sciences & Engineering, Technion, Israel. To Amir Grau and Ariel Shemesh from Biomedical Core Facility at Rappaport Faculty of Medicine, Technion, Israel.

Sivan Raviv was supported by the Kaplan Family Fellowship for Exceptional Women.

Mohammed Alyan was supported by the Frances Brody Fellowship.

Author 1 and Author 2 contributed equally to this work.

## Appendix A. Supplementary data

Supplementary data to this article can be found online at https://doi.

org/10.1016/j.jconrel.2022.03.028.

## References


[1] B. Moldoveanu, et al., Inflammatory mechanisms in the lung, J. Inflamm. Res. 2 (2009) 1–11.
[2] Mark D Siege, Acute Respiratory Distress Syndrome: Epidemiology, Pathophysiology, Pathology, and Etiology in Adults, UpToDate, 2022.
[3] André F Rendeiro, et al., The spatial landscape of lung pathology during COVID-19 progression, Nature 593 (7860) (2021) 564–569, https://doi.org/10.1038/s41586-021-03475-6.
[4] T.N. Lilah Lopez, Graham Weber, Katlyn Kleimola, Megan Bereda, Yiling Liu, Emma K. Accorsi, Steven J. Skates, John P. Santa Maria Jr., Kendal R. Smith, Mark Kalinich, Seroprevalence of anti-SARS-CoV-2 IgG antibodies in the staff of a public school system in the midwestern United States, PLoS One 16 (2021), https://doi.org/10.1371/journal.pone.0243676.
[5] E. Fan, D. Brodie, A.S. Slutsky, Acute respiratory distress syndrome: advances in diagnosis and treatment, JAMA 319 (2018) 698–710, https://doi.org/10.1001/jama.2017.21907.
[6] M. Diamond, P. F. H, D. Sanghavi, et al., Acute Respiratory Distress Syndrome. https://www.ncbi.nlm.nih.gov/books/NBK436002/>.
[7] M.A.M. e al, Acute respiratory distress syndrome, Nat. Rev. Dis. Prim. 5 (2019).
[8] C. Rosales, C.A. Lowell, M. Schnoor, E. Uribe-Querol, Neutrophils: their role in innate and adaptive immunity 2017, J Immunol Res 2017 (2017) 9748345, https://doi.org/10.1155/2017/9748345.
[9] H.B. Frieboes, S. Raghavan, B. Godin, Modeling of nanotherapy response as a function of the tumor microenvironment: focus on liver metastasis, Front. Bioeng. Biotechnol. 8 (2020), https://doi.org/10.3389/fbioe.2020.01011.
[10] F.O. Martinez, S. Gordon, The M1 and M2 paradigm of macrophage activation: time for reassessment, F1000Prime Rep. 6 (2014) 13, https://doi.org/10.12703/p6-13.
[11] U. Saqib, et al., Phytochemicals as modulators of M1-M2 macrophages in inflammation, Oncotarget 9 (2018) 17937–17950, https://doi.org/10.18632/oncotarget.24788.
[12] Anne Lodge, Ask A Scientist: What's the Difference Between M1 and M2 Macrophages?. https://cellero.com/blog/ask-scientist-whats-difference-m1-m2-macrophages/>, 2020.
[13] S. Arora, K. Dev, B. Agarwal, P. Das, M.A. Syed, Macrophages: their role, activation and polarization in pulmonary diseases, Immunobiology 223 (2018) 383–396, https://doi.org/10.1016/j.imbio.2017.11.001.
[14] D.S. Chi, M. Qui, G. Krishnaswamy, C. Li, W. Stone, Regulation of nitric oxide production from macrophages by lipopolysaccharide and catecholamines, Nitric Oxide 8 (2003) 127–132, https://doi.org/10.1016/S1089-8603(02)00148-9.
[15] R.S. Flannagan, G. Cosío, S. Grinstein, Antimicrobial mechanisms of phagocytes and bacterial evasion strategies, Nat. Rev. Microbiol. 7 (2009) 355–366, https://doi.org/10.1038/nrmicro2128.
[16] L. Pandolfi, et al., Broncho-alveolar inflammation in COVID-19 patients: a correlation with clinical outcome, BMC Pulm. Med. 20 (2020) 301, https://doi.org/10.1186/s12890-020-01343-z.
[17] P.E. Marik, G.U. Meduri, P.R. Rocco, D. Annane, Glucocorticoid treatment in acute lung injury and acute respiratory distress syndrome, Crit. Care Clin. 27 (2011) 589–607, https://doi.org/10.1016/j.ccc.2011.05.007.
[18] G.U. Meduri, et al., Methylprednisolone infusion in early severe ARDS: results of a randomized controlled trial, Chest 131 (2007) 954–963, https://doi.org/10.1378/chest.06-2100.
[19] M. Jing Liu, Xiaobin Zheng, Yiying Huang, Hong Shan, Jin Huang, Successful use of methylprednisolone for treating severe COVID-19, J. Allergy Clin. Immunol. 146 (2020) 325–327, https://doi.org/10.1016/j.jaci.2020.05.021.
[20] Kaitlin M. Landolf, S. M. L, Christina Rose, Jackie P. Johnston, Christopher D. Adams, Jerry Altshuler, Karen Berger, Deepali Dixit, Muhammad K. Effendi, Mojdeh S. Heavner, Diana Lemieux, Audrey J. Littlefield, Andrea M. Nei, Kent A. Owusu, Marisa Rinehart, Blake Robbins, Ginger E. Rouse, Melissa L. Thompson Bastin, Corticosteroid use in ARDS and its application to evolving therapeutics for coronavirus disease 2019 (COVID-19): a systematic review, J. Am. Coll. Clin. Pharm. (2021), https://doi.org/10.1002/phar.2637.
[21] P.J. Barnes, How corticosteroids control inflammation: quintiles prize lecture 2005, Br. J. Pharmacol. 148 (2006) 245–254, https://doi.org/10.1038/sj.bjp.0706736.
[22] J.S. Sloka, M. Stefanelli, The mechanism of action of methylprednisolone in the treatment of multiple sclerosis, Mult. Scler. 11 (2005) 425–432, https://doi.org/10.1191/1352458505ms1190oa.
[23] A. Stern, et al., Corticosteroids for pneumonia, Cochrane Database Syst. Rev. 12 (2017), https://doi.org/10.1002/14651858.CD007720.pub3. Cd007720.
[24] M. Oray, K. Abu Samra, N. Ebrahimiadib, H. Meese, C.S. Foster, Long-term side effects of glucocorticoids, Expert Opin. Drug Saf. 15 (2016) 457–465, https://doi.org/10.1517/14740338.2016.1140743.
[25] B. Pedre, U. Barayeu, D. Ezeriņa, T.P. Dick, The mechanism of action of N-acetylcysteine (NAC): the emerging role of H2S and sulfane sulfur species, Pharmacol. Ther. 228 (2021), 107916, https://doi.org/10.1016/j.pharmthera.2021.107916.
[26] Y. Liu, et al., Mucus production stimulated by IFN-AhR signaling triggers hypoxia of COVID-19, Cell Res. 30 (2020) 1078–1087, https://doi.org/10.1038/s41422-020-00435-z.
[27] P. Santus, et al., Oxidative stress and respiratory system: pharmacological and clinical reappraisal of N-acetylcysteine, Copd 11 (2014) 705–717, https://doi.org/10.3109/15412555.2014.898040.
[28] K. Dua, et al., Increasing complexity and interactions of oxidative stress in chronic respiratory diseases: an emerging need for novel drug delivery systems, Chem. Biol. Interact. 299 (2019) 168–178, https://doi.org/10.1016/j.cbi.2018.12.009.
[29] A.M. Sadowska, J. Verbraecken, K. Darquennes, W.A. De Backer, Role of N-acetylcysteine in the management of COPD, Int. J. Chron. Obstruct. Pulmon. Dis. 1 (2006) 425–434, https://doi.org/10.2147/copd.2006.1.4.425.
[30] Y. Zhang, et al., Effects of N-acetylcysteine treatment in acute respiratory distress syndrome: a meta-analysis, Exp. Ther. Med. 14 (2017) 2863–2868, https://doi.org/10.3892/etm.2017.4891.
[31] M. a H.p.R. Agency, Intravenous N-Acetylcysteine (NAC) for Paracetamol Overdose: Reminder of Authorised Dose Regimen; Possible Need for Continued Treatment with NAC, 2017.
[32] M. Tenório, N.G. Graciliano, F.A. Moura, A.C.M. Oliveira, M.O.F. Goulart, N-Acetylcysteine (NAC): impacts on human health, Antioxidants (Basel) 10 (2021), https://doi.org/10.3390/antiox10060967.
[33] V. Kapustina, S. Ovcharenko, P. Litvicki, High doses of N-acetylcysteine alone or in combination with inhaled corticosteroids and oxidative stress in patients with COPD, Eur. Respir. J. 38 (2011), p3911.
[34] R.G.a.S.S. Madhusudanan Pallavi, Hydrogel systems and their role in neural tissue engineering, J. R. Soc. Interface 17 (2020), https://doi.org/10.1098/rsif.2019.0505.
[35] A. Akbarzadeh, et al., Liposome: classification, preparation, and applications, Nanoscale Res. Lett. 8 (2013) 102, https://doi.org/10.1186/1556-276X-8-102.
[36] P.O. Nkadi, T.A. Merritt, D.A. Pillers, An overview of pulmonary surfactant in the neonate: genetics, metabolism, and the role of surfactant in health and disease, Mol. Genet. Metab. 97 (2009) 95–101, https://doi.org/10.1016/j.ymgme.2009.01.015.
[37] W. Abate, A.A. Alghaithy, J. Parton, K.P. Jones, S.K. Jackson, Surfactant lipids regulate LPS-induced interleukin-8 production in A549 lung epithelial cells by inhibiting translocation of TLR4 into lipid raft domains, J. Lipid Res. 51 (2010) 334–344, https://doi.org/10.1194/jlr.M000513.
[38] M.B. Fessler, R.S. Summer, Surfactant lipids at the host-environment interface. Metabolic sensors, suppressors, and effectors of inflammatory lung disease, Am. J. Respir. Cell Mol. Biol. 54 (2016) 624–635, https://doi.org/10.1165/rcmb.2016-0011PS.
[39] M. Mohamed, et al., PEGylated liposomes: immunological responses, Sci. Technol. Adv. Mater. 20 (2019) 710–724, https://doi.org/10.1080/14686996.2019.1627174.
[40] T.T. Tai, et al., A strategy to treat COVID-19 disease with targeted delivery of inhalable liposomal hydroxychloroquine: a preclinical pharmacokinetic study, Clin Transl Sci 14 (2021) 132–136, https://doi.org/10.1111/cts.12923.
[41] M.P. Lokugamage, et al., Optimization of lipid nanoparticles for the delivery of nebulized therapeutic mRNA to the lungs, Nat. Biomed. Eng. 5 (2021) 1059–1068, https://doi.org/10.1038/s41551-021-00786-x.
[42] J. Zhang, et al., Amikacin liposome inhalation suspension (ALIS) penetrates non-tuberculous mycobacterial biofilms and enhances amikacin uptake into macrophages, Front. Microbiol. 9 (2018), https://doi.org/10.3389/fmicb.2018.00915.
[43] A. Schroeder, A. Sigal, K. Turjeman, Y. Barenholz, Using PEGylated nano-liposomes to target tissue invaded by a foreign body, J. Drug Target. 16 (2008) 591–595, https://doi.org/10.1080/10611860802228939.
[44] G.B. Olga, Intratracheal versus intravenous liposomal delivery of siRNA, antisense oligonucleotides and anticancer drug, Pharm. Res. 26 (2008), https://doi.org/10.1007/s11095-008-9755-4.
[45] B.D. Anderson, V. Taphouse, Initial rate studies of hydrolysis and acyl migration in methylprednisolone 21-hemisuccinate and 17-hemisuccinate, J. Pharm. Sci. 70 (1981) 181–186, https://doi.org/10.1002/jps.2600700217.
[46] E.M. Mathew, A. Ravi, N. Rameshwar, M. Sudheer, B. Krishnamurthy, Development and validation of an analytical method for related substances in N-acetyl–L-cysteine effervescent tablets by RP-HPLC, J. Pharm. Educ. Res. 51 (4) (2017) 626–635.
[47] J.R. Bellare, D. H. T. D, L.E. Scriven, Y. Talmon, Controlled environment vitrification system: an improved sample preparation technique, J. Electron Microsc. Tech. 10 (1988) 87–111, https://doi.org/10.1002/jemt.1060100111.
[48] Y. Talmon, The study of nanostructured liquids by cryogenic-temperature electron microscopy — a status report, J. Mol. Liq. 210 (2015) 2–8, https://doi.org/10.1016/j.molliq.2015.03.054.
[49] Y. Cao, et al., Punicalagin prevents inflammation in LPS-induced RAW264.7 macrophages by inhibiting FoxO3a/autophagy signaling pathway, Nutrients 11 (2019) 2794, https://doi.org/10.3390/nu11112794.
[50] M. Naito, et al., Structural tuning of oligonucleotides for enhanced blood circulation properties of unit polyion complexes prepared from two-branched poly (ethylene glycol)-block-poly(l-lysine), J. Control. Release 330 (2021) 812–820, https://doi.org/10.1016/j.jconrel.2021.01.001.
[51] S.A. Valente, et al., Polysaccharide-based formulations as potential carriers for pulmonary delivery – a review of their properties and fates, Carbohydr. Polym. 118784 (2021), https://doi.org/10.1016/j.carbpol.2021.118784.
[52] R. Veldhuizen, K. Nag, S. Orgeig, F. Possmayer, The role of lipids in pulmonary surfactant, Biochim. Biophys. Acta (BBA) - Mol. Basis Dis. 1408 (1998) 90–108, https://doi.org/10.1016/S0925-4439(98)00061-1.
[53] R.U. Yuval Avnir, Veronica Wasserman, Simcha Even-Chen, Maya Broyer, Yechezkel Barenholz, Yaakov Naparstek, Amphipathic weak acid glucocorticoid prodrugs remote-loaded into sterically stabilized nanoliposomes evaluated in

arthritic rats and in a beagle dog, Arthritis Rheum. 58 (2007) 119–129, https://doi.org/10.1002/art.23230.
[54] A. Tonks, et al., Dipalmitoylphosphatidylcholine modulates inflammatory functions of monocytic cells independently of mitogen activated protein kinases, Clin. Exp. Immunol. 124 (2001) 86–94, https://doi.org/10.1046/j.1365-2249.2001.01479.x.
[55] Y. Samuni, S. Goldstein, O.M. Dean, M. Berk, The chemistry and biological activities of N-acetylcysteine, Biochim. Biophys. Acta 1830 (2013) 4117–4129, https://doi.org/10.1016/j.bbagen.2013.04.016.
[56] F. Pan, L. Han, Y. Zhang, Y. Yu, J. Liu, Optimization of Caco-2 and HT29 co-culture in vitro cell models for permeability studies, Int. J. Food Sci. Nutr. 66 (2015) 680–685, https://doi.org/10.3109/09637486.2015.1077792.
[57] J.Y. Lock, T.L. Carlson, R.L. Carrier, Mucus models to evaluate the diffusion of drugs and particles, Adv. Drug Deliv. Rev. 124 (2018) 34–49, https://doi.org/10.1016/j.addr.2017.11.001.
[58] L.E. Morgan, et al., Disulfide disruption reverses mucus dysfunction in allergic airway disease, Nat. Commun. 12 (2021) 249, https://doi.org/10.1038/s41467-020-20499-0.
[59] F.R. D'Alessio, Mouse models of acute lung injury and ARDS, in: Methods in Molecular Biology, 2018, pp. 341–350, https://doi.org/10.1007/978-1-4939-8570-8_22.
[60] Tyler C. Vandivort, Dowon An, William C. Parks, An Improved Method for Rapid Intubation of the Trachea in Mice. http://www.jove.com/video/53771>, 2016.
[61] H. Ibaraki, et al., In vivo fluorescence imaging of passive inflammation site accumulation of liposomes via intravenous administration focused on their surface charge and PEG modification, Pharmaceutics 13 (2021), https://doi.org/10.3390/pharmaceutics13010104.
[62] H.C. Kazunori Igarashi, Taehun Hong, Yasutaka Anraku, Fotios Mpekris, Triantafyllos Stylianopoulos, Thahomina Khan, Akira Matsumoto, Kazunori Kataoka, Yu Matsumoto, Tatsuya Yamasoba, Vascular Bursts Act as a Versatile Tumor Vessel Permeation Route for Blood-Borne Particles and Cells, 2021, https://doi.org/10.1002/smll.202103751.

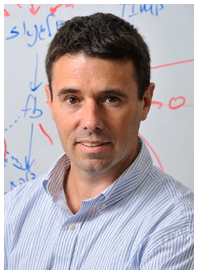

**Avi Schroeder**

**Sivan Arber Raviv**

**Mohammed Alyan**